Influence of torsional rigidity of flexible appendages on the dynamics of spacecrafts

Masakatsu Chiba[*] and Hidetake Magata

*Department of Aerospace Engineering, Graduate School of Engineering,
Osaka Prefecture University, 1-1 Gakuen-cho, Naka-ku, Sakai, Osaka 599-8531, Japan*

Abstract. The influence of torsional rigidity of hinged flexible appendage on the linear dynamics of flexible spacecrafts with liquid on board was analyzed by considering the spacecraft's main body as a rigid tank, its flexible appendages as two elastically supported elastic beams, and the onboard liquid as an ideal liquid. The meniscus of the liquid free surface due to surface tension was considered. Using the Lagrangian of the spacecraft's main body (rigid tank), onboard liquid, and two beams (flexible appendages) in addition to assuming the system moved symmetrically, the coupled system frequency equations were obtained by applying the Rayleigh-Ritz method. The influence of the torsional rigidity of the flexible appendages on the spacecraft's coupled vibration characteristics was primary focus of investigation. It was found that coupled vibration modes especially that of appendage considerably changed with torsion spring parameter κ_t of the flexible appendage. In addition, variation of the main body displacement with system parameters was investigated.

Keywords: hydroelastic vibration; space structure; coupled system; liquid sloshing; zero-gravity; elastic supported; torsional spring

1. Introduction

Because large space structures need to be lightweight, they have low structural rigidity, which causes them to vibrate easily at low frequencies. Thus, thruster injection for attitude control or orbit modification may cause vibrations in flexible appendages, such as antennas and solar arrays, as well as onboard liquids such as wastewater and fuel. This leads to the development of strong coupled vibrations that affect the dynamic behavior of the structure's main body, which pose a serious problem for high-attitude satellites requiring accurate positioning, such as those used for precise astronomical photography. Therefore, clarifying the dynamic interaction behavior of flexible space structures with liquid onboard is crucial for improving space structure stability and reliability.

Several researchers have theoretically examined how liquids slosh in containers in low-gravity environments. For example, Abramson (1996) reviewed studies conducted to that point. Bauer *et al.* (1990a, b) conducted two free vibration analyses of liquids in a cylindrical or rectangular vessel

---

[*]Corresponding author, Professor, E-mail: chiba@aero.osakafu-u.ac.jp

accounting for liquid meniscus due to surface tension. Agrawal (1993) used a boundary layer model to analyze the dynamic behavior of liquid in a rotating space vehicle. Komatsu (1999) theoretically investigated a space vehicle's tank sloshing frequency by using a mechanical model and obtained natural frequencies via a semi-empirical formula using potential flow models. Chiba *et al.* (2002) investigated coupled natural vibrations of a liquid, and the elastic membrane bottom of a rigid-walled cylindrical container. Utsumi (2004) proposed mechanical models for the sloshing of liquids in a tear-shaped axisymmetric tank. Yuanjun *et al.* (2007) conducted a nonlinear analysis of sloshing liquid in a cylindrical container. This analysis considered the shape of the static meniscus shape in low-gravity environments with an energy method that used pitching excitation around the cylinder's center of gravity. Berglund *et al.* (2007) used a pulse-suppression approach to control liquid propellant sloshing in a Delta IV rocket. Li *et al.* (2011) proposed an equivalent mechanical model for liquid sloshing during draining which represented time varying property of liquid sloshing. Recently, Yong and Baozeng (2017) presented a simulation of large-amplitude three-dimensional liquid sloshing in a spherical tank.

McIntyre *et al.* (1982) studied how sloshing affects spacecraft motion by investigating the stability of an oblate spinning body with liquid fuel aboard. Santini *et al.* (1978, 1983) derived equations of motion for an orbiting spacecraft containing a sloshing liquid in a plane rigid tank and discussed the spacecraft's stability. Lü *et al.* (2005) studied pitching motion under gravity of a two-dimensional rectangular tank with elastic appendages. From the numerical simulations, they found that the coupling of elastic appendages with rigid tanks are effective in high gravity conditions, while the coupling of liquid fuel and rigid tanks are effective in low gravity conditions. Gasbarri *et al.* (2016) presented a dynamic model of spacecraft with a solar panel and considered fuel sloshing using multi-body approach. They employed a pendulum model for the fuel sloshing, and clarified the interaction among the control, the attitude dynamics, the flexibility of the solar array and the sloshing motion of the spacecraft. For spacecrafts with multiple propellant tanks, Baozeng *et al.* (2015) presented a coupled dynamic model using Lagrange's equation, and Zhou and Huang (2015) presented a constrained surface model in which they clarified the coupling dynamics between the spacecraft and the propellant sloshing in tanks.

A recent study (Chiba *et al.* 2013) served as the first step toward clarifying fundamental vibration characteristics of liquid-containing flexible space structures by proposing a mechanical model and analyzing the axisymmetric coupled vibrations of a flexible structure containing liquid. The proposed model treated the main body as a rigid mass, its flexible appendages as two elastic beams, and the onboard liquid as a "spring-mass" system (mechanical model). The mechanical model adopted a single liquid sloshing mode (i.e., fundamental sloshing mode), which helped determine the coupled system's fundamental vibration characteristics, i.e., the main body-flexible appendages-liquid system.

The second step in clarifying fundamental vibration characteristics was taken by Chiba and Magata (2017), who studied how liquid sloshing influenced the dynamics of a flexible space structure containing a liquid. They accomplished this by considering the spacecraft's main body a rigid tank, its flexible appendages as two elastic beams, and the liquid onboard as an ideal liquid with respect to the meniscus of the free surface due to surface tension.

In the previous studies (2013, 2017), a spacecraft model was considered in which two flexural appendages were rigidly connected to the main spacecraft body. Flexible appendages fixed to the spacecraft main body must have enough strength against disturbance during orbital or attitude control of the spacecraft, and they must be designed to avoid transmitting those disturbances from the appendages due to thermal-snap, for example. In this study, we model the flexibility of the root

(a) Cylindrical tank with two elastically-supported beams

(b) Liquid in cylindrical tank
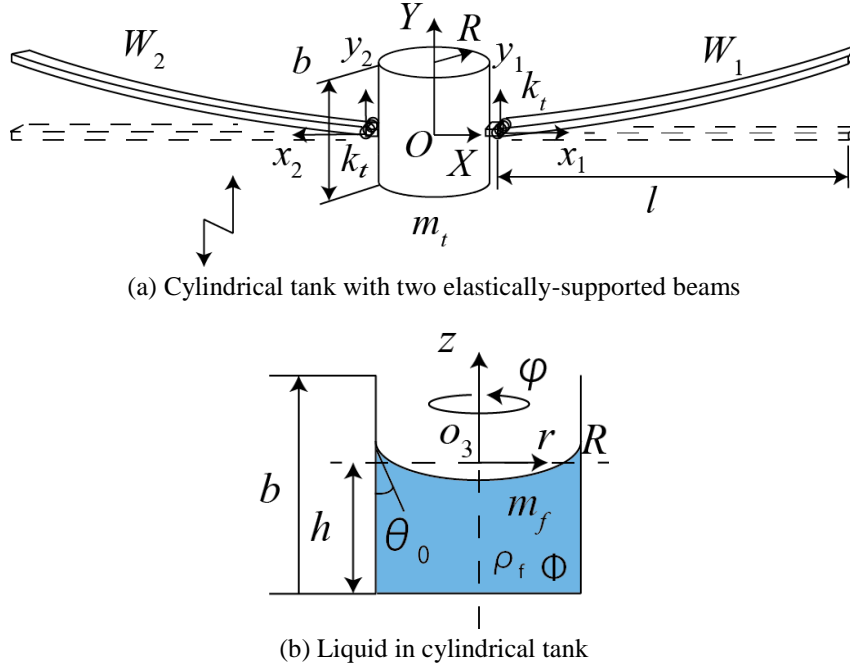
Fig. 1 Flexible spacecraft model with liquid tank

of the flexible appendages as a torsional spring, and in the third step in this clarification process, we study the spacecraft model that includes the torsional rigidity of the roots of two flexible appendages.

2. Basic equations and boundary conditions

2.1 Analytical model

Fig. 1 shows small amplitude free vibration of a spacecraft with flexible appendages, such as solar arrays, on both sides of the main body, which contains a liquid. In the model, the spacecraft's main body is considered as a rigid cylindrical tank, with two elastically supported elastic beams representing flexible appendages, and a liquid on board. The tank's radius, length, and mass are represented by R, b, and m_t, respectively, and its displacement is represented by Y_M in the inertia coordinate $o - XY$. The elastic beams are modeled as uniform Euler-Bernoulli beams, each with a length of l, cross-sectional area of A, density of ρ_b, Young's modulus of E, second moment of area of I, and displacements corresponding to $W_1(x_1, t)$ and $W_2(x_2, t)$. The beams are also elastically supported with torsional spring constant k_t. The onboard liquid is treated as an inviscid ideal liquid with a density of ρ_f and a mass of $m_f = \pi R^2 h \rho_f$, where h denotes the height of the liquid when ignoring its meniscus. The liquid's velocity potential, $\Phi(r, \varphi, z, t)$, is given in the coordinate system, $o - rz\varphi$, which has its origin located on a flat liquid surface. In microgravity, surface

tension is the predominant force on a liquid, producing an axisymmetric meniscus $z_0(r)$ with a contact angle with respect to a side wall of θ_0 as shown in Fig. 1(b). Therefore, we represent the liquid's free surface as $Z_f(r, \varphi, t) = z_0(r) + Z(r, \varphi, t)$.

We assume a symmetric arrangement with respect to the rigid tank for the beams and that the tank's center of mass is on the mid-surface of the beams. These assumptions enabled axisymmetric in-plane motion, i.e., movement along the upward and downward directions in the plane only under a small amplitude vibration. Here, we investigate the effect of the elastic torsional support of the two beams.

2.2 Basic equations and boundary conditions

2.2.1 Liquid

We assume the liquid to be incompressible and inviscid and to exhibit irrotational motion. The basic equations and boundary conditions are as follows (see Chiba *et al.* 2017)

Laplace equation

$$\Delta\Phi = \frac{\partial^2\Phi}{\partial r^2} + \frac{1}{r}\frac{\partial\Phi}{\partial r} + \frac{\partial^2\Phi}{\partial z^2} = 0 \tag{1}$$

Kinematic condition on the free surface

$$\frac{\partial\Phi}{\partial z} - \frac{\partial Z}{\partial t} - \frac{\partial z_0(r)}{\partial r}\frac{\partial\Phi}{\partial r} = 0 \qquad at \ \ z = z_0(r) \tag{2}$$

Dynamic condition on the free surface

$$\rho_f\frac{\partial\Phi}{\partial t} - \frac{\sigma}{r}\frac{\partial}{\partial r}\left[r\left\{1 - \left(\frac{r\cos\theta_0}{R}\right)^2\right\}^{3/2}\frac{\partial Z}{\partial r}\right] = -\rho_f\ddot{Y}_M(t)z \qquad at \ \ z = z_0(r) \tag{3}$$

Boundary conditions

$$\frac{\partial\Phi}{\partial z} = 0 \qquad at \ \ z = -h \tag{4}$$

$$\frac{\partial\Phi}{\partial r} = 0 \qquad at \ \ r = R \tag{5}$$

Contact angle

$$\frac{\partial Z}{\partial r} = 0 \qquad at \ \ r = R \tag{6}$$

Conservation of liquid volume

$$\int_0^{2\pi}\int_0^R Z(r, \varphi, t)\, r\, dr\, d\varphi = 0 \tag{7}$$

Meniscus of the free surface (represented by Bauer *et al.* 1990b)

$$z_0(r) = \frac{2R\left(1 - \sin^3\theta_0\right)}{3\cos^3\theta_0} - \frac{R}{\cos\theta_0}\sqrt{1 - \left(\frac{r\cos\theta_0}{R}\right)^2} \tag{8}$$

2.2.2 Beams

We modeled the beams with torsional supported mass-free boundary conditions. Therefore, the beam's shearing force at the end, with mass attached, is in balance with the inertia force of the mass. The beam's bending moment is in balance with the moment of the torsional spring (torsional spring constant k_t). In contrast, at the free end, both the shearing force and bending moment are zero

$$x_i = 0: \qquad \text{shearing force:} \qquad -\frac{1}{2}M\ddot{Y}_M(t) - EI\frac{\partial^3 W_i}{\partial x_i^3} = 0 \tag{9}$$

$$\text{bending moment:} \qquad EI\frac{\partial^2 W_i}{\partial x_i^2} - k_t\frac{\partial W_i}{\partial x_i} = 0 \tag{10}$$

$$x_i = l: \qquad \text{shearing force:} \qquad -EI\frac{\partial^3 W_i}{\partial x_i^3} = 0 \tag{11}$$

$$\text{bending moment:} \qquad -EI\frac{\partial^2 W_i}{\partial x_i^2} = 0 \tag{12}$$

2.3 Lagrangian of the system

2.3.1 Lagrangian of the liquid

The Lagrangian of the liquid, L_f, is defined as (see Chiba *et al.* 2017)

$$L_f = \frac{1}{2}m_f\dot{Y}_M^2 + \int_0^R\int_0^{2\pi}\left\{\rho_f\frac{\partial\Phi}{\partial t} - \frac{\sigma}{r}\frac{\partial}{\partial r}\left[r\left\{1 - \left(\frac{r\cos\theta_0}{R}\right)^2\right\}^{3/2}\frac{\partial Z}{\partial r}\right] + \rho_f\ddot{Y}_M(t)z\right\}Z\,rdrd\varphi \tag{13}$$

$$at\ \ z = z_0(r)$$

2.3.2 Lagrangian of the beams and main body

The kinetic energies of the beams and main body (tank) are defined as follows

$$T = \frac{1}{2}m_t\dot{Y}_M^2 + \frac{1}{2}\rho_b A\int_0^l\left(\dot{W}_1\right)^2 dx_1 + \frac{1}{2}\rho_b A\int_0^l\left(\dot{W}_2\right)^2 dx_2 \tag{14}$$

The beams and the main body both have potential energy consisting of the stain energy of the beams and the two torsional springs.

$$U = \frac{1}{2} EI \int_0^l \left(\frac{\partial^2 W_1}{\partial x_1^2} \right)^2 dx_1 + \frac{1}{2} EI \int_0^l \left(\frac{\partial^2 W_2}{\partial x_2^2} \right)^2 dx_2 + \frac{1}{2} k_t \left(\frac{\partial W_1}{\partial x_1} \bigg|_{x_1=0} \right)^2 + \frac{1}{2} k_t \left(\frac{\partial W_2}{\partial x_2} \bigg|_{x_2=0} \right)^2 \tag{15}$$

Thus, the total Lagrangian, L_{tb}, is

$$\begin{aligned} L_{tb} = &\frac{1}{2} m_t \dot{Y}_M^2 + \frac{1}{2} \rho_b A \int_0^l \left(\dot{W}_1 \right)^2 dx_1 + \frac{1}{2} \rho_b A \int_0^l \left(\dot{W}_2 \right)^2 dx_2 \\ &- \frac{1}{2} EI \int_0^l \left(\frac{\partial^2 W_1}{\partial x_1^2} \right)^2 dx_1 - \frac{1}{2} EI \int_0^l \left(\frac{\partial^2 W_2}{\partial x_2^2} \right)^2 dx_2 - \frac{1}{2} k_t \left(\frac{\partial W_1}{\partial x_1} \bigg|_{x_1=0} \right)^2 - \frac{1}{2} k_t \left(\frac{\partial W_2}{\partial x_2} \bigg|_{x_2=0} \right)^2 \end{aligned} \tag{16}$$

2.4 Non-dimensionalization

Here we introduce non-dimensional parameters and non-dimensionalize the previous equations.

$$\tau = \omega_b t, \ \omega_b = \sqrt{\frac{EI}{\rho_b A l^4}}, \ \Omega = \frac{\omega}{\omega_b}, \ \phi = \frac{\Phi}{\omega_b R^2}, \ \xi_i = \frac{x_i}{l}, \ \rho = \frac{r}{R}, \ \eta = \frac{z}{R}, \ y_M = \frac{Y_M}{l}, \ \kappa_t = \frac{k_t l}{EI}$$

$$\zeta = \frac{Z}{R}, \ \eta_0 = \frac{z_0}{R}, \ w_i = \frac{W_i}{l} \ (i = 1, 2), \ \bar{\beta} = \frac{\pi R^2}{2A}, \ \lambda = \frac{l}{R}, \ \bar{\rho} = \frac{\rho_f}{\rho_b}, \ h_0 = \frac{h}{R}, \ \gamma = \frac{\sigma A l}{EI} \tag{17}$$

$$\bar{m}_t = \frac{m_t}{2\rho_b A l}, \ \bar{m}_f = \frac{m_f}{2\rho_b A l} = \frac{\bar{\rho}\bar{\beta}h_0}{\lambda}, \ \bar{M} = \bar{m}_t + \bar{m}_f, \ \bar{L}_f = \frac{L_f \lambda^2}{\rho_b A l^3 \omega_b^2}, \ \bar{L}_{tb} = \frac{L_f \lambda^2}{\rho_b A l^3 \omega_b^2}$$

The most significant parameters of these are the tank mass ratio $\bar{M}$, the cross-sectional area ratio $\bar{\beta}$ of the beams and rigid tank, the aspect ratio λ of beam length and tank radius, the surface tension parameter γ, the liquid height ratio h_0, the density ratio $\bar{\rho}$, and the torsional spring parameter κ_t. The dot represents derivatives with respect to t and the dash represents derivatives with respect to τ as

$$\dot{k} = \frac{dk}{dt} = \frac{dk}{d(\tau / \omega_b)} = \omega_b \frac{dk}{d\tau} = \omega_b k' \tag{18}$$

2.4.1 Non-dimensionalized equations for liquid

$$\Delta \phi = 0 \tag{1'}$$

$$\frac{\partial \phi}{\partial \eta} - \frac{\partial \zeta}{\partial \tau} - \frac{\partial \eta_0 (\rho)}{\partial \rho} \frac{\partial \phi}{\partial \rho} = 0 \quad at \ \eta = \eta_0 (\rho) \tag{2'}$$

$$\frac{\partial \phi}{\partial \tau} - \frac{\lambda^3 \gamma}{\bar{\rho}} \frac{1}{\rho} \frac{\partial}{\partial \rho} \left[\rho \left\{ 1 - \left(\rho \cos \theta_0 \right)^2 \right\}^{3/2} \frac{\partial \zeta}{\partial \rho} \right] = -\lambda y_M'' \eta_0 \tag{3'}$$

$$\frac{\partial \phi}{\partial \eta} = 0 \quad at \ \ \eta = -h_0 \tag{4'}$$

$$\frac{\partial \phi}{\partial \rho} = 0 \quad at \ \ \rho = 1 \tag{5'}$$

$$\frac{\partial \zeta}{\partial \rho} = 0 \quad at \ \ \rho = 1 \tag{6'}$$

$$\int_0^{2\pi} \int_0^1 \zeta\left(\rho, \varphi, \tau\right) \rho d\rho d\phi = 0 \tag{7'}$$

$$\eta_0\left(\rho\right) = \frac{2\left(1 - \sin^3 \theta_0\right)}{3\cos^3 \theta_0} - \frac{1}{\cos \theta_0}\sqrt{1 - \left(\rho \cos \theta_0\right)^2} \tag{8'}$$

2.4.2 Non-dimensionalized boundary conditions for beams

$$\xi_i = 0: \ \ \bar{M}\, y_M'' + \frac{\partial^3 w_i}{\partial \xi_i^3} = 0 \ , \qquad \frac{\partial^2 w_i}{\partial \xi_i^2} - \kappa_t \frac{\partial w_i}{\partial \xi_i} = 0 \tag{9', 10'}$$

$$\xi_i = 1: \ \ \frac{\partial^3 w_i}{\partial \xi_i^3} = 0, \qquad \frac{\partial^2 w_i}{\partial \xi_i^2} = 0 \tag{11', 12'}$$

2.4.3 Non-dimensionalized Lagrangian
Liquid:

$$\bar{L}_f = \lambda^2 \bar{m}_f\, y_M'^2 + \frac{2\bar{\beta}\bar{\rho}}{\pi \lambda} \int_0^1 \int_0^{2\pi} \left\{ \frac{\partial \phi}{\partial \tau} - \frac{\lambda^3 \gamma}{\bar{\rho}} \frac{1}{\rho} \frac{\partial}{\partial \rho}\left[\rho \left\{ 1 - \left(\rho \cos \theta_0\right)^2 \right\}^{3/2} \frac{\partial \zeta}{\partial \rho} \right] + \lambda\, y_M'' \eta_0 \right\} \zeta \rho d\rho d\varphi \atop at \ \ \eta = \eta_0(\rho) \tag{13'}$$

Rigid tank and beams:

$$\bar{L}_{tb} = \lambda^2 \left\{ \begin{array}{l} \bar{m}_t\, y_M'^2 + \dfrac{1}{2}\displaystyle\int_0^1 w_1'^2 d\xi_1 + \dfrac{1}{2}\displaystyle\int_0^1 w_2'^2 d\xi_2 \\[12pt] -\dfrac{1}{2}\displaystyle\int_0^1 \left(\dfrac{\partial^2 w_1}{\partial \xi_1^2}\right)^2 d\xi_1 - \dfrac{1}{2}\displaystyle\int_0^1 \left(\dfrac{\partial^2 w_2}{\partial \xi_2^2}\right)^2 d\xi_2 - \dfrac{\kappa_t}{2}\left(\left.\dfrac{\partial w_1}{\partial \xi_1}\right|_{\xi_1=0}\right)^2 - \dfrac{\kappa_t}{2}\left(\left.\dfrac{\partial w_2}{\partial \xi_2}\right|_{\xi_2=0}\right)^2 \end{array} \right\} \tag{16'}$$

3. Method of solutions

We assume that the system exhibits small amplitude vibrations with a non-dimensional circular frequency, Ω, as follows

$$
\begin{aligned}
y_M(\tau) &= \bar{w}(0)\cos\Omega\tau \\
\phi(\rho,\eta,\tau) &= -\Omega\bar{\phi}(\rho,\eta)\sin\Omega\tau \\
\zeta(\rho,\tau) &= \bar{\zeta}(\rho)\cos\Omega\tau \\
w_i(\xi_i,\tau) &= \bar{w}_i(\xi_i)\cos\Omega\tau \quad (i=1,2)
\end{aligned}
\tag{19}
$$

where the rigid tank's displacement equals that of the beam root at $\xi_i = 0$.

3.1 Lagrangian of the system

By substituting Eq. (19) into the Lagrangians in Eqs. (13)' and (16)' and integrating for a period of vibration, $\tau = 0 - 2\pi/\Omega$, we obtain,

Liquid:

$$
\begin{aligned}
\tilde{L}_f = {}&\lambda^2 \bar{m}_f \Omega^2 \bar{w}(0)^2 \\
&- \frac{2\bar{\beta}\bar{\rho}}{\pi\lambda}\int_0^1\int_0^{2\pi}\left\{\Omega^2\bar{\phi} + \frac{\lambda^3\gamma}{\bar{\rho}}\frac{1}{\rho}\frac{\partial}{\partial\rho}\left[\rho\{1-(\rho\cos\theta_0)^2\}^{3/2}\frac{\partial\bar{\zeta}}{\partial\rho}\right] + \lambda\Omega^2\eta_0\bar{w}(0)\right\}\bar{\zeta}\rho\,d\rho\,d\varphi \\
&\hspace{9cm} at \ \ \eta = \eta_0(\rho)
\end{aligned}
\tag{20}
$$

where

$$
\tilde{L}_f = \frac{\Omega}{\pi}\int_0^{2\pi/\Omega}\bar{L}_f\,d\tau
\tag{21}
$$

and

$$
\int_0^{2\pi/\Omega}\sin^2\Omega\tau\,d\tau = \int_0^{2\pi/\Omega}\cos^2\Omega\tau\,d\tau = \frac{\pi}{\Omega}
\tag{22}
$$

were used.

Rigid tank and beams:

$$
\tilde{L}_{tb} = \lambda^2\left\{
\begin{aligned}
&\bar{m}_t\bar{w}(0)^2\Omega^2 + \frac{1}{2}\Omega^2\int_0^1(\bar{w}_1)^2\,d\xi_1 + \frac{1}{2}\Omega^2\int_0^1(\bar{w}_2)^2\,d\xi_2 \\
&- \frac{1}{2}\int_0^1\left(\frac{\partial^2\bar{w}_1}{\partial\xi_1^2}\right)^2 d\xi_1 - \frac{1}{2}\int_0^1\left(\frac{\partial^2\bar{w}_2}{\partial\xi_2^2}\right)^2 d\xi_2 - \frac{\kappa_t}{2}\left(\frac{\partial w_1}{\partial\xi_1}\bigg|_{\xi_1=0}\right)^2 - \frac{\kappa_t}{2}\left(\frac{\partial w_2}{\partial\xi_2}\bigg|_{\xi_2=0}\right)^2
\end{aligned}
\right\}
\tag{23}
$$

where

$$\tilde{L}_{tb} = \frac{\Omega}{\pi} \int\limits_0^{2\pi/\Omega} \bar{L}_{tb} \, d\tau \tag{24}$$

3.2 Liquid velocity potential and liquid surface displacement

The liquid velocity potential, $\bar{\phi}(\rho,\eta)$, which satisfies Eq. (1)' and boundary condition Eqs. (1)' to (8)', and the liquid surface displacement, $\bar{\zeta}(\rho)$, are defined in the following (see Chiba *et al.* 2017)

$$\bar{\phi}(\rho,\eta) = \sum_d A_{0d} J_0(\varepsilon_{0d}\rho) \frac{\cosh[\varepsilon_{0d}(\eta+h_0)]}{\cosh(\varepsilon_{0d}h_0)} \tag{25}$$

$$\bar{\zeta}(\rho) = \sum_e a_{0e} J_0(\varepsilon_{0e}\rho) \tag{26}$$

where ε_{0d} satisfies the following equations

$$J'_0(\varepsilon_{0d})\left(= -J_1(\varepsilon_{0d})\right) = 0 \tag{27}$$

Substituting Eqs. (25) and (26) into Eq. (20), we calculate the Lagrangian of the liquid as

$$\tilde{L}_f = \lambda^2 \bar{m}_f \Omega^2 \bar{y}_M^2 - \frac{4\bar{\beta}\bar{\rho}}{\lambda} \sum_i \sum_j A_{0j} \varepsilon_{0j} \left(C_{4ji} - C_{5ji}\right) \left[\begin{array}{l} \sum_d A_{0d} \left\{ \Omega^2 \tilde{C}_{1di} + \dfrac{\lambda^3 \gamma}{\bar{\rho}} \varepsilon_{0d} \sum_e (C_{4de} - C_{5de}) \tilde{C}_{2ei} \right\} \\ + \lambda \Omega^2 \, \bar{y}_M \tilde{C}_{3i} \end{array} \right] \tag{28}$$

where

$$\tilde{C}_{1di} = \frac{C_{1di}}{\chi_{0i}} = \int_0^1 \frac{\cosh[\varepsilon_{0d}(\eta_0(\rho)+h_0)]}{\cosh(\varepsilon_{0d}h_0)} J_0(\varepsilon_{0d}\rho) J_0(\varepsilon_{0i}\rho) \rho \, d\rho \tag{29}$$

$$\tilde{C}_{2ei} = \frac{C_{2ei}}{\chi_{0i}} = -\varepsilon_{0i}\varepsilon_{0e} \int_0^1 \rho \left\{1 - (\rho\cos\theta_0)^2\right\}^{3/2} J'_0(\varepsilon_{0e}\rho) J'_0(\varepsilon_{0i}\rho) \, d\rho \tag{30}$$

$$\tilde{C}_{3i} = \frac{C_{3i}}{\chi_{0i}} = \int_0^1 \eta_0(\rho) J_0(\varepsilon_{0i}\rho) \rho \, d\rho \tag{31}$$

$$C_{4dn} = \chi_{0n} \int_0^1 \frac{\sinh[\varepsilon_{0d}\{\eta_0(\rho)+h_0\}]}{\cosh(\varepsilon_{0d}h_0)} J_0(\varepsilon_{0d}\rho) J_0(\varepsilon_{0n}\rho) \rho \, d\rho \tag{32}$$

$$C_{5dn} = \chi_{0n} \int_0^1 \frac{\rho\cos\theta_0}{\sqrt{1 - (\rho\cos\theta_0)^2}} \frac{\cosh[\varepsilon_{0d}\{\eta_0(\rho)+h_0\}]}{\cosh(\varepsilon_{0d}h_0)} J'_0(\varepsilon_{0d}\rho) J_0(\varepsilon_{0n}\rho) \rho \, d\rho \tag{33}$$

where

$$\chi_{0i} = \frac{2}{J_0^2\left(\varepsilon_{0i}\right)}$$

3.3 Displacement of beams

If we assume that the two beams are identical and have symmetric displacement, the displacement of the beams can be determined as

$$\bar{w}_i\left(\xi_i\right) = \sum_m C_m \tilde{w}_m\left(\xi_i\right), \quad i = 1,2 \tag{34}$$

where $\tilde{w}_m\left(\xi_i\right)$ is an eigenfunction of a beam with a torsional supported mass-free boundary condition.

$$
\begin{aligned}
\tilde{w}_m(\xi_i) = \cosh\alpha_m\xi_i &+ \frac{\left(1+\bar{M}\kappa_t\right)\cos\alpha_m - \left(1-\bar{M}\kappa_t\right)\cosh\alpha_m - 2\bar{M}\alpha_m\sin\alpha_m}{D_m}\alpha_m\sinh\alpha_m\xi_i \\
&+ \frac{2\kappa_t\cosh\alpha_m + \left(1+\bar{M}\kappa_t\right)\alpha_m\sinh\alpha_m - \left(1-\bar{M}\kappa_t\right)\alpha_m\sin\alpha_m}{D_m}\cos\alpha_m\xi_i \\
&+ \frac{\left(1-\bar{M}\kappa_t\right)\cos\alpha_m - \left(1+\bar{M}\kappa_t\right)\cosh\alpha_m - 2\bar{M}\alpha_m\sinh\alpha_m}{D_m}\alpha_m\sin\alpha_m\xi_i
\end{aligned}
\tag{35}
$$

where

$$D_m = 2\kappa_t\cos\alpha_m + \left(1-\bar{M}\kappa_t\right)\alpha_m\sinh\alpha_m - \left(1+\bar{M}\kappa_t\right)\alpha_m\sin\alpha_m \tag{36}$$

and α_m satisfies the following frequency equation

$$\left(\kappa_t - \alpha_m^2\bar{M}\right)\tan\alpha + \left(\kappa_t + \alpha_m^2\bar{M}\right)\tanh\alpha_m + \left(1+\bar{M}\kappa_t\right)\alpha_m - \frac{\left(1-\bar{M}\kappa_t\right)\alpha_m}{\cosh\alpha_m\cos\alpha_m} = 0 \tag{37}$$

$$\alpha_m^2 = \sqrt{\frac{\rho_b A l^4}{EI}}\omega = \Omega \tag{38}$$

which is a function of tank mass ratio $\bar{M}$ and torsional spring parameter κ_t.

By substituting Eq. (34) into Eq. (23) we obtain

$$\tilde{L}_{tb} = \lambda^2 \left\{
\begin{aligned}
&\bar{m}_t\Omega^2\sum_m\sum_n C_m C_n \tilde{w}_{1m}(0)\tilde{w}_{1n}(0) + \Omega^2\sum_m\sum_n C_m C_n X_{mn}^{00} - \sum_m\sum_n C_m C_n X_{mn}^{22} \\
&- \kappa_t\sum_m\sum_n C_m C_n \tilde{w}_m'(0)\tilde{w}_n'(0)
\end{aligned}
\right\}
\tag{39}$$

where

$$X_{mn}^{00} = \int_0^1 \tilde{w}_m(\xi)\,\tilde{w}_n(\xi)\,\mathrm{d}\xi = \begin{cases} -\bar{M}\tilde{w}_m(0)\,\tilde{w}_n(0) & : m \neq n \\ \dfrac{1}{4}\left\{ \tilde{w}_n^2(1) - 3\bar{M}\tilde{w}_n^2(0) + \dfrac{\kappa_t}{\alpha_n^4}\,\tilde{w}_n'^2(0)\right\} & : m = n \end{cases} \tag{40}$$

$$X_{mn}^{22} = \int_0^1 \frac{\mathrm{d}^2 \tilde{w}_m(\xi)}{\mathrm{d}\xi^2}\frac{\mathrm{d}^2 \tilde{w}_n(\xi)}{\mathrm{d}\xi^2}\,\mathrm{d}\xi = \begin{cases} -\kappa_t \tilde{w}_m'(0)\,\tilde{w}_n'(0) & : m \neq n \\ \dfrac{1}{4}\alpha_n^4\left\{ \tilde{w}_n^2(1) - \bar{M}\tilde{w}_n^2(0) + \dfrac{3\kappa_t}{\alpha_n^4}\,\tilde{w}_n'^2(0)\right\} & : m = n \end{cases} \tag{41}$$

In Eqs. (39) through (41), the dash represents the derivative with respect to ξ.

3.4 Lagrangian of the total system

Finally, we defined the Lagrangian for the entire system as

$$\begin{aligned} \tilde{L} &= \tilde{L}_f + \tilde{L}_{tb} \\ &= \lambda^2 \left\{ \begin{aligned} &\left(\bar{m}_f + \bar{m}_t\right)\Omega^2 \sum_m \sum_n C_m C_n \tilde{w}_{1m}(0)\tilde{w}_{1n}(0) \\ &- \frac{4\bar{\beta}\bar{\rho}}{\lambda^3}\sum_i \sum_j A_{0j}\varepsilon_{0j}\left(C_{4ji} - C_{5ji}\right)\left[\begin{aligned} &\sum_d A_{0d}\left\{\Omega^2 \tilde{C}_{1di} + \frac{\lambda^3 \gamma}{\bar{\rho}}\varepsilon_{0d}\sum_e (C_{4de} - C_{5de})\tilde{C}_{2ei}\right\} \\ &+ \lambda\Omega^2\,\bar{y}_M\,\tilde{C}_{3i} \end{aligned}\right] \\ &+ \Omega^2 \sum_m \sum_n C_m C_n X_{mn}^{00} - \sum_m \sum_n C_m C_n X_{mn}^{22} - \kappa_t \sum_m \sum_n C_m C_n \tilde{w}_m'(0)\tilde{w}_n'(0) \end{aligned}\right\} \end{aligned} \tag{42}$$

$$\begin{aligned} \tilde{\tilde{L}} &= \left(\bar{m}_f + \bar{m}_t\right)\Omega^2 \sum_m \sum_n C_m C_n \tilde{w}_{1m}(0)\tilde{w}_{1n}(0) \\ &\quad - \frac{4\bar{\beta}\bar{\rho}}{\lambda^3}\sum_i \sum_j A_{0j}\varepsilon_{0j}\left(C_{4ji} - C_{5ji}\right)\left[\begin{aligned} &\sum_d A_{0d}\left\{\Omega^2 \tilde{C}_{1di} + \frac{\lambda^3 \gamma}{\bar{\rho}}\varepsilon_{0d}\sum_e (C_{4de} - C_{5de})\tilde{C}_{2ei}\right\} \\ &+ \lambda\Omega^2\,\bar{y}_M\,\tilde{C}_{3i} \end{aligned}\right] \\ &\quad + \Omega^2 \sum_m \sum_n C_m C_n X_{mn}^{00} - \sum_m \sum_n C_m C_n X_{mn}^{22} - \kappa_t \sum_m \sum_n C_m C_n \tilde{w}_m'(0)\tilde{w}_n'(0) \end{aligned} \tag{43}$$

3.5 Rayleigh-Ritz method

We then applied the *Rayleigh-Ritz* method to obtain the following minimalized condition for $\tilde{\tilde{L}}$:

$$\frac{\partial \tilde{\tilde{L}}}{\partial A_{0j}} = 0,\ \frac{\partial \tilde{\tilde{L}}}{\partial B_m} = 0 \tag{44}$$

$$\frac{\partial \tilde{\tilde{L}}}{\partial A_{0j}} = -\frac{4\bar{\beta}\bar{\rho}}{\lambda^3}\sum_{i}\left[\sum_{d}A_{0d}\left\{\begin{array}{l}\varepsilon_{0j}\left(C_{4ji}-C_{5ji}\right)\left(\Omega^2\tilde{C}_{1di}+\frac{\lambda^3\gamma}{\bar{\rho}}\varepsilon_{0d}\sum_{e}\left(C_{4de}-C_{5de}\right)\tilde{C}_{2ei}\right)\\[2mm]+\varepsilon_{0d}\left(C_{4di}-C_{5di}\right)\left(\Omega^2\tilde{C}_{1ji}+\frac{\lambda^3\gamma}{\bar{\rho}}\varepsilon_{0j}\sum_{e}\left(C_{4je}-C_{5je}\right)\tilde{C}_{2ei}\right)\end{array}\right\}\\[4mm]+\lambda\varepsilon_{0j}\left(C_{4ji}-C_{5ji}\right)\Omega^2\tilde{C}_{3i}\sum_{m}B_{m}\tilde{w}_{m}(0)\end{array}\right] = 0 \qquad (45)$$

$$\frac{\partial \tilde{\tilde{L}}}{\partial B_m} = 2\bar{M}\Omega^2\sum_{n}B_n\tilde{w}_{1m}(0)\tilde{w}_{1n}(0) + 2\Omega^2\sum_{n}B_n X_{mn}^{00} - 2\sum_{n}B_n X_{mn}^{22}$$

$$-2\kappa_t\sum_{n}B_n\tilde{w}_{m}'(0)\tilde{w}_{n}'(0) - \Omega^2\frac{4\bar{\beta}\bar{\rho}}{\lambda^2}\sum_{i}\sum_{j}A_{0j}\varepsilon_{0j}\left(C_{4ji}-C_{5ji}\right)\tilde{C}_{3i}\tilde{w}_{m}(0) = 0 \qquad (46)$$

The equation in a matrix form is described as

$$\left\{\begin{pmatrix}\boldsymbol{K}_1 & \boldsymbol{0}\\ \boldsymbol{0} & \boldsymbol{K}_4\end{pmatrix} - \Omega^2\begin{pmatrix}\boldsymbol{M}_1 & \boldsymbol{M}_2\\ \boldsymbol{M}_3 & \boldsymbol{M}_4\end{pmatrix}\right\}\begin{Bmatrix}\boldsymbol{A}_{0d}\\ \boldsymbol{B}_n\end{Bmatrix} = \boldsymbol{0} \qquad (d=1,2,\cdots l, \quad n=1,2,\cdots,k) \qquad (47)$$

where

$$K_{1jd} = -2\bar{\beta}\gamma\sum_{i}\sum_{e}\left\{\begin{array}{l}\varepsilon_{0j}\left(C_{4ji}-C_{5ji}\right)\varepsilon_{0d}\left(C_{4de}-C_{5de}\right)\tilde{C}_{2ei}\\[2mm]+\varepsilon_{0d}\left(C_{4di}-C_{5di}\right)\varepsilon_{0j}\left(C_{4je}-C_{5je}\right)\tilde{C}_{2ei}\end{array}\right\} \qquad :l\times l$$

$$K_{4mn} = -X_{mn}^{22} - \kappa_t\tilde{w}_{m}'(0)\tilde{w}_{n}'(0) \qquad :k\times k$$

$$M_{1jd} = \frac{2\bar{\beta}\bar{\rho}}{\lambda^3}\sum_{i}\left\{\varepsilon_{0j}\left(C_{4ji}-C_{5ji}\right)\tilde{C}_{1di} + \varepsilon_{0d}\left(C_{4di}-C_{5di}\right)\tilde{C}_{1ji}\right\} \qquad :l\times l$$

$$M_{2jm} = \frac{2\bar{\beta}\bar{\rho}}{\lambda^2}\tilde{w}_{m}(0)\varepsilon_{0j}\sum_{i}\left(C_{4ji}-C_{5ji}\right)\tilde{C}_{3i} \qquad :l\times k$$

$$M_{3mj} = \frac{2\bar{\beta}\bar{\rho}}{\lambda^2}\tilde{w}_{m}(0)\varepsilon_{0j}\sum_{i}\left(C_{4ji}-C_{5ji}\right)\tilde{C}_{3i} \qquad :k\times k$$

$$M_{4mn} = -\bar{M}\tilde{w}_{m}(0)\tilde{w}_{n}(0) - X_{mn}^{00} \qquad :k\times k$$

$$(d=1,2,\cdots,l, \quad j=1,2,\cdots,l, \quad m=1,2,\cdots,k, \quad n=1,2,\cdots,k)$$

(48)

We obtained the coupled natural circular frequency as eigenvalues and the vibration modes as eigenvectors using these equations.

4. Numerical results

4.1 Coupled system without liquid

We first considered a coupled spacecraft system with an empty tank, corresponding to a spacecraft running out of fuel. The relevant system parameters in this case are $\bar{m}_t$ $(=\bar{M})$ and κ_t.
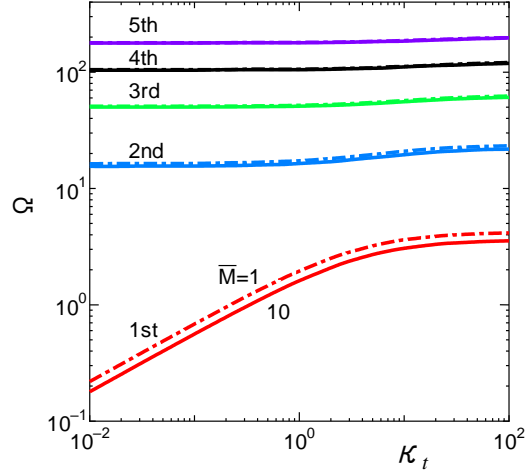
Fig. 2 Natural circular frequency with torsional spring parameter κ_t (without liquid: $\bar{M} = 1, 10$)

(a) $\kappa_t = 0.01$ (b) $\kappa_t = 0.1$ (c) $\kappa_t = 1$ (d) $\kappa_t = 10$ (e) $\kappa_t = 100$
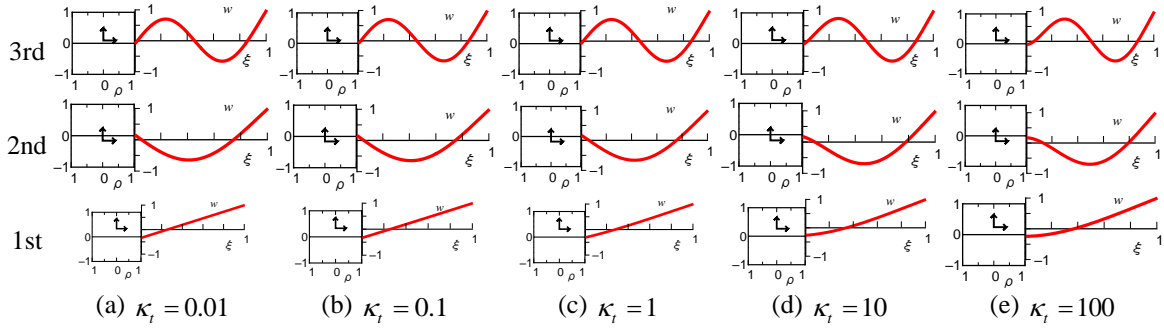
Fig. 3 Vibration mode with torsional spring parameter κ_t (without liquid: $\bar{M} = 1$); (a) κ_t=0.01; (b) κ_t=0.1; (c) κ_t=1; (d) κ_t=10; (e) κ_t=100

4.1.1 Influence of κ_t on natural circular frequency

Fig. 2 shows the natural circular frequency variations of the lowest five modes with κ_t. Because κ_t is defined as κ_t=$k_t l/EI$, an increase in κ_t corresponds to an increase in the torsional spring constant (keeping the beam's length, l, constant), or an increase in beam length, l, (keeping κ_t constant). In the figure, solid and single-dotted lines correspond to results for $\bar{M} = 10$ and 1, respectively. We found that as κ_t increases, the natural circular frequencies also increase and tend to the values when the beam is clamped ($\Omega = 3.52,\ 22.03,\ 61.70$ when $\bar{M} \to \infty$) (see, Chiba *et al.* 2017).

4.1.2 Influence of κ_t on vibration mode

Fig. 3 shows the lowest three vibration modes for κ_t=0.01, 0.1, 1, 10, 100 when $\bar{M} = 1$. In Fig. 3, a square indicates the spacecraft's main body (cylindrical tank), the red curve indicates the right-hand side beam's vibration mode, the crossing point of the two small arrows indicates the inertia frame origin, and the distance of the crossing point from the tank's center indicates the tank's displacement. In addition, the displacements of tank y_M and beam w are normalized such that their maximum of which is unity.

When κ_t=0.01 (Fig. 3(a)), the beam's boundary condition is almost "simply supported," which is a condition where the beam has relatively rigid body motion without bending, as well as a large deflection angle, which renders an extremely low natural frequency as shown in Fig. 2. As κ_t increases, boundary conditions tend toward a clamped condition and the deflection angle becomes zero accordingly natural frequency increases.

The movement of tank y_M is large in the first mode and decreases with higher vibration modes. In addition, the tank's displacement differs when vibration modes are of odd or even order. Although Fig. 3 shows the case when $\bar{M}=1$, results of the cases where $\bar{M}=10, 100$ had similar tendencies for the effect of κ_t.

4.1.3 Influence of κ_t on tank displacement

Variations in y_M for a wider value of κ_t when $\bar{M}=1$ are shown in Fig. 4(a). As mentioned, y_M values of the first and the third modes are in a negative direction, whereas that of the second mode is in a positive direction. On the left-hand and the right-hand sides of Fig. 4(a), we show the vibration modes when κ_t=10^{-4} in Fig. 4(b) and those when κ_t=10^4 in Fig. 4(c).

The magnitudes of y_M differ with vibration mode, i.e., as κ_t increases, the displacement of y_M for the first mode decreases, whereas those of the second and third modes slightly increase.

4.2 Coupled system

Next, we considered the coupled spacecraft system with liquid onboard. The system parameters in this case are contact angle θ_0, liquid height ratio h_0, density ratio $\bar{\rho}$, surface tension parameter γ, aspect ratio λ, area ratio $\bar{\beta}$, mass ratio $\bar{m}_t$, and torsional spring parameter κ_t.

4.2.1 Influence of κ_t on coupled natural circular frequency

Fig. 5 shows coupled natural circular frequency variations with κ_t. The coupled natural circular frequency curves that have predominant liquid motion are constant with κ_t, whereas those with predominant beam motions increase with κ_t (see Fig. 2). The intersection of these curves occurs at some values of κ_t, exhibiting the exchange of vibration modes, i.e., marked regions.

4.2.2 Influence of κ_t on coupled vibration mode

Fig. 6 identifies coupled system vibration modes in the κ_t range shown in a red circle in Fig. 5. In this case, vibration amplitudes of liquid surface $\bar{\zeta}/\lambda$, tank displacement y_M, and beam deflection w are normalized such that the maximum of which is unity. In Fig. 6 we see the intersection of two natural frequency curves occurring at $1.65 \leq \kappa_t \leq 1.70$ (Figs. 6(b), 6(c)), and an exchange of the vibration modes occurs. These results are for the θ_0=90° case, in which one cannot see coupling between liquid and beam motions near the cross region (see, Chiba *et al.* 2017).

4.2.3 Influence of κ_t on displacement of tank

Fig. 7 shows y_M variation for the first and second modes when θ_0=90°. Vibration mode exchange occurs at κ_t, which is indicated by a single-dotted line in the figure. The natural frequency curve, in which beam vibration is predominant, is shown as a red thick line, whereas that in which free surface vibration is predominant is shown as a thin blue line, and is nearly zero along the whole κ_t range. We see that the tank does not move in a coupled vibration where liquid
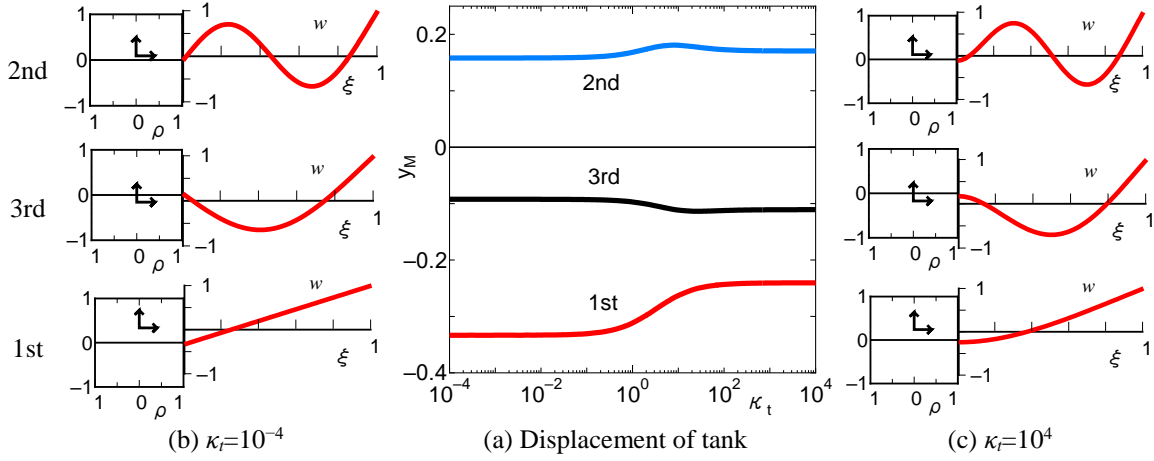
Fig. 4 Variation of displacement of tank y_M and vibration mode with torsional spring parameter κ_t (without liquid $\bar{M} = 1$)

motion is predominant, whereas the tank moves in a coupled vibration in which beam vibration is predominant.

4.2.4 Variation of natural frequency with liquid height

Fig. 8 shows natural circular frequency variations with liquid height h_0 when $\theta_0=60°$, $90°$, $100°$ ($\bar{\rho}=1$, $\gamma=10^{-4}$, $\bar{\beta}=10$, $\lambda=10$, $\bar{m}_t=1$, $\kappa_t=1$). The frequency curve with a dashed line corresponds to the coupled frequency where beam motion is predominant, whereas curves with solid lines correspond to coupled frequencies in which the liquid mode is predominant. As h_0 decreases, these two frequency curves cross.

4.2.5 Influence of liquid height on the displacement of tank

Fig. 9 shows tank displacement y_M variations with liquid height h_0 for three contact angles, $\theta_0=60°$, $90°$, $100°$, which correspond to the first and second modes when $\kappa_t=1$. Single-dotted vertical lines correspond to the h_0 value in which two natural frequency curves cross. We found that displacement y_M drastically changes near the crossing region when $\theta_0=60°$ and $100°$ in the vibration mode in which liquid sloshing is predominant. When the κ_t value is small, i.e., $\kappa_t=1$, the liquid fuel is consumed throughout the spacecraft's mission. Additionally, the two types of coupled frequencies, especially those with the lowest sloshing modes, approach each other, producing movement of the main body (tank).

5. Conclusions

The influence of the torsional rigidity of the hinged flexible appendage on the dynamics of liquid-containing flexible space structures was analyzed by considering a spacecraft's main body as a rigid tank, its flexible appendages as two elastically supported elastic beams, and the liquid on board as an ideal liquid, considering the meniscus of the liquid free surface. The obtained results are summarized as follows:
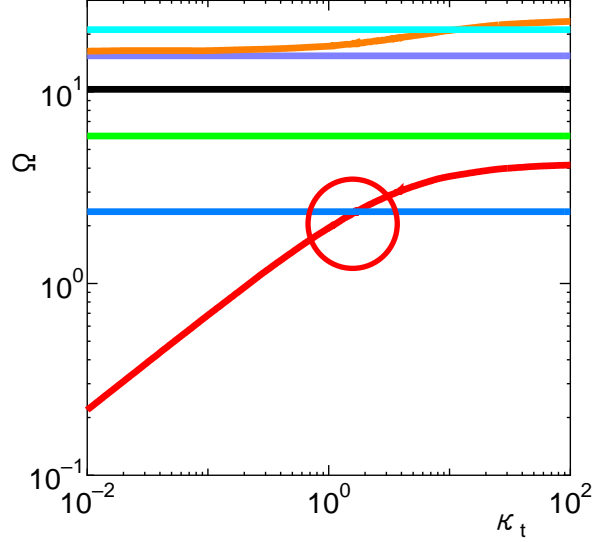
Fig. 5 Natural circular frequency with torsional spring parameter κ_t: $\theta_0 = 90°$, $h_0 = 1$, $\bar{\rho} = 1$, $\gamma = 10^{-4}$, $\bar{\beta} = 10$, $\lambda = 10$, $\bar{m}_t = 1$

(a) $\kappa_t = 1.6$ (b) $\kappa_t = 1.65$ (c) $\kappa_t = 1.7$ (d) $\kappa_t = 1.75$ (e) $\kappa_t = 1.8$
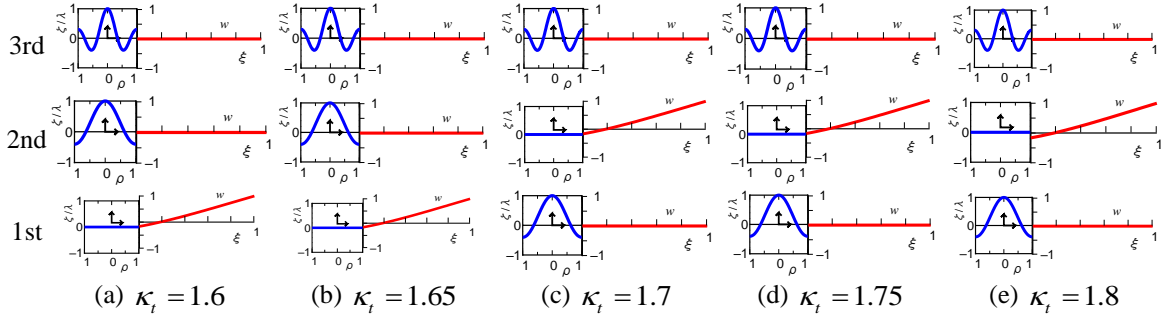
Fig. 6 Vibration mode with torsional spring parameter κ_t: $\theta_0 = 90°$, $h_0 = 1$, $\bar{\rho} = 1$, $\gamma = 10^{-4}$, $\bar{\beta} = 10$, $\lambda = 10$, $\bar{m}_t = 1$

i) System without liquid

• Natural frequency and vibration mode

As $\bar{M}$ increased, natural frequency decreased. When κ_t is small, the natural vibration mode trends toward that of a simple support-free beam and has rigid body motion, and has very low frequency. With an increase in κ_t, the boundary condition of the beam tends toward that of a "clamp-free" beam and the natural frequency increases.

• Displacement of spacecraft main body

For each vibration mode, tank displacement decreases as $\bar{M}$ increases, and the amplitude becomes small for higher vibration modes. The tank displacement change of direction opposes that of the beam tip direction for odd order modes and is the same direction as that for even vibration modes. The effect of κ_t on tank displacement depends on the vibration mode, i.e., it decreases with κ_t for the first mode, but slightly increases with κ_t for the second and third modes.
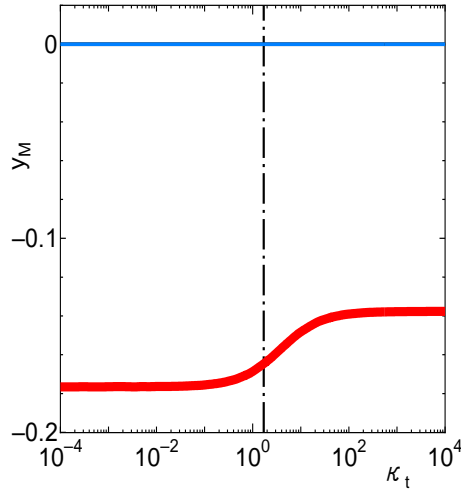
Fig. 7 Displacement of tank y_M with torsional spring parameter κ_t: $\theta_0 = 90°$, $h_0 = 1$, $\bar{\rho} = 1$, $\gamma = 10^{-4}$, $\bar{\beta} = 10$, $\lambda = 10$, $\bar{m}_t = 1$

(a) $\theta_0 = 60°$ (b) $\theta_0 = 90°$ (c) $\theta_0 = 100°$
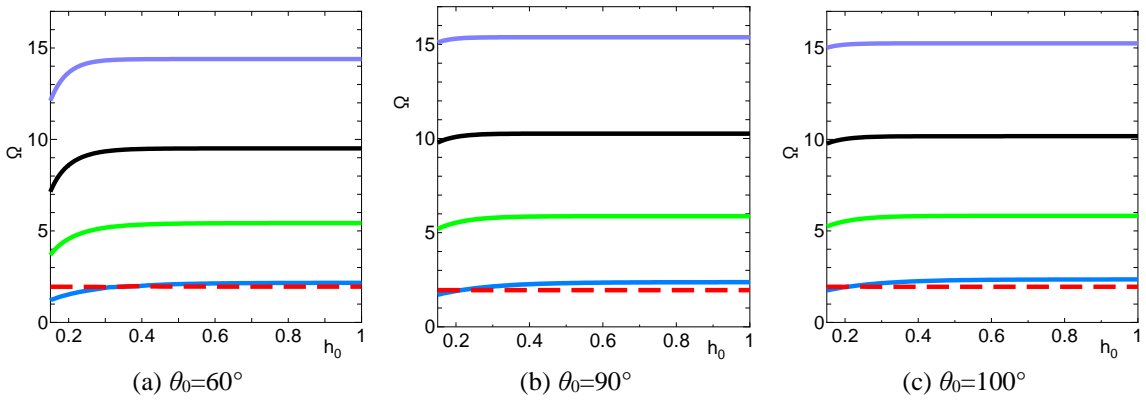
Fig. 8 Natural circular frequency with liquid height h_0: $\bar{\rho} = 1$, $\gamma = 10^{-4}$, $\bar{\beta} = 10$, $\lambda = 10$, $\bar{m}_t = 1$, $\kappa_t = 1$

(a) $\theta_0 = 60°$ (b) $\theta_0 = 90°$ (c) $\theta_0 = 100°$
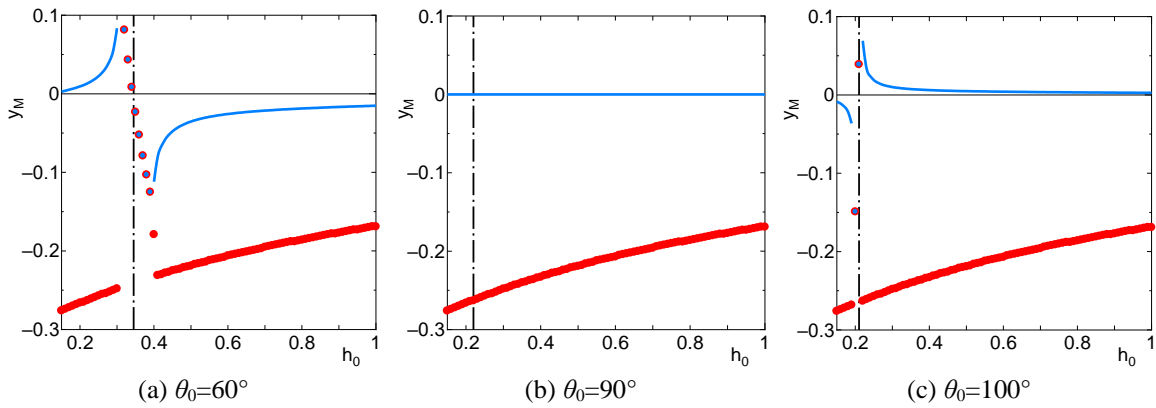
Fig. 9 Displacement of tank y_M with liquid height h_0: $\bar{\rho} = 1$, $\gamma = 10^{-4}$, $\bar{\beta} = 10$, $\lambda = 10$, $\bar{m}_t = 1$, $\kappa_t = 1$

ii) Coupled system
• Coupled natural frequency

Depending on κ_t, two types of coupled natural frequencies approach each other, which produce the coupling of liquid sloshing and beam vibration.

• Tank displacement

When $\theta = 90°$ tank displacement is zero in the coupled sloshing mode and not zero in the coupled beam mode. When $\theta_0 = 60°$ and $100°$, tank displacement is close to zero even in the coupled sloshing mode.

When κ_t is small, i.e., $\kappa_t = 1$, the volume of liquid fuel in the spacecraft decreases over the duration of the mission, and the two types of coupled frequencies, especially during the lowest sloshing mode, approach each other, producing the movement of the main body (tank).

The authors believe that the above results will assist to qualitatively understand the effect of rigidity of appendage roots on the coupled natural vibration characteristics of a flexural spacecraft with a liquid on board. This data may prove important in the future spacecraft design.

Acknowledgements

References

Abramson, H.N. (1966), *The Dynamic Behavior of Liquids in Moving Containers*, Chapter 11, NASA SP-106.

Agrawal, B.N. (1993), "Dynamic characteristics of liquid motion in partially filled tanks of a spinning spacecraft", *J. Guid. Contr. Dyn.*, **16**(4), 636-640.

Baozeng, Y., Wenjun, W. and Yulong, Y. (2016), "Modelling and coupling dynamics of the spacecraft with multiple propellant tanks", *AIAA J.*, **54**(11), 3608-3618.

Bauer, H.F and Eidel, W. (1990a), "Linear liquid oscillations in cylindrical container under zero gravity", *Appl. Micrograv. Tech.*, **2**, 212-220.

Bauer, H.F and Eidel, W. (1990b), "Small amplitude liquid oscillations in a rectangular container under zero gravity", *Zeitsschrift fur Flugwissenschaften und Weltraumforschung*, **14**(1-2), 1-8.

Berglund, M.D., Bassett, C.E., Kelso, J.M., Mishic, J. and Schrange, D. (2007), "The boeing delta IV launch vehicle-pulse-settling approach for second-stage hydrogen propellant management", *Acta Astronaut.*, **61**(1-6), 416-424.

Chiba, M., Chiba, S. and Takemura, K. (2013), "Coupled hydroelastic vibrations of a liquid on flexible space structures under zero-gravity-part I. mechanical model", *Coupled Syst. Mech.*, **2**(4), 303-327.

Chiba, M. and Magata, H. (2017), "Influence of liquid sloshing on dynamics of flexible space structures", *J. Sound Vibr.*, **401**, 1-22.

Chiba, M., Watanabe, H. and Bauer, H.F. (2002), "Hydroelastic coupled vibrations in a cylindrical container with a membrane bottom, containing liquid with surface tension", *J. Sound Vibr.*, **251**(4), 717-740.

Gasbarri, P., Sabatini, M. and Pisculli, A. (2016), "Dynamic modelling and stability parametric analysis of a flexible spacecraft with fuel slosh", *Acta Astronaut.*, **127**, 141-159.

Komatsu, K. (1999), "Modeling of the dynamic behavior of liquids in spacecraft", *Int. J. Micrograv. Sci. Appl.*, **16**(3), 182-190.

Lü, J., Li, L.J. and Wang, T. (2005), "Dynamic response of liquid filled rectangular tank with elastic appendages under pitching excitation", *Appl. Math. Mech.*, **28**(3), 351-359.

Li, Q., Ma, X. and Wang, T. (2011), "Equivalent mechanical model for liquid sloshing during draining", *Acta Astronaut*., **68**(1-2), 91-100.

McIntyre, J.E. and McIntyre, J.M. (1982), "Some effects of propellant motion on the performance of spinning satellites", *Acta Astronaut*., **9**(12), 645-661.

Santini, P. and Barboni, R. (1978), "Motion of orbiting spacecrafts with a sloshing fluid", *Acta Astronaut*., **5**(7-8), 467-490.

Santini, P. and Barboni, R. (1983), "A minicomputer finite elements program for microgravity hydroelastic analysis", *Acta Astronaut*., **10**(2), 81-90.

Utsumi, M. (2004), "A mechanical model for low-gravity sloshing in an axisymmetric tank", *Trans. ASME, J. Appl. Mech*., **71**(5), 724-730.

Young, T. and Baozeng, Y. (2017), "Simulation of large-amplitude three dimensional liquid sloshing in spherical tanks", *AIAA J.,* **55**(6), 2052-2059.

Yuanjun, H., Xingrui, M., Pigping, W. and Benli, W. (2007), "Low-gravity liquid nonlinear sloshing analysis in a tank under pitching excitation", *J. Sound Vibr*., **299**(1-2), 164-177.

Zhou, Z. and Huang, H. (2015), "Constraint surface model for large amplitude sloshing of the spacecraft with multiple tanks", *Acta Astronaut*., **111**, 222-229.

CC

Nomenclature (Non-dimensional)

A	Beam cross-sectional area
b	Tank length
E	Young's modulus of beam
h	Equivalent liquid height : $\left(h_0 = h / R \right)$
I	Beam second moment of area
k_t	Torsional spring constant $\left(\kappa_t = k_t l / EI \right)$
l	Beam length $\left(\lambda = l / R \right)$
m_f	Liquid mass : $(\bar{m}_f = m_f / 2\rho_b Al)$
m_t	Rigid tank mass : $(\bar{m}_t = m_t / 2\rho_b Al)$
M	Total of m_f and m_t : $(\bar{M} = \bar{m}_f + \bar{m}_t)$
$O - XY$	Spacecraft coordinate system
$\text{o} - r\varphi z$	Tank coordinate system : $(\text{o} - \rho\varphi\eta)$

R Tank radius

t Time : $(\tau = \omega_b t)$

Y_M Rigid tank displacement : $(y_M = Y_M / l)$

$W_i(x_i, t)$ Beam displacements : $(w_i = W_i / l)$

$Z(r, \varphi, t)$ Liquid surface displacement : $(\zeta = Z / R)$

$z_0(r)$ Static liquid free surface : $(\eta_0 = z_0 / R)$

$Z_f(r, \varphi, t)$ Liquid free surface displacement

$\Phi(r, \varphi, z, t)$ Liquid velocity potential : $(\phi = \Phi / \omega_b R^2)$

$\bar{\beta}$ Beam and tank area ratio $(= \pi R^2 / 2A)$

θ_0 Static contact angle of liquid

ρ_f Liquid density

ρ_b Beam density

σ Coefficient of free surface tension : $(\gamma = \sigma R^2 l / EI)$

$\bar{\rho}$ Density ratio $(= \rho_f / \rho_b)$

ξ_i Non-dimensional coordinate : $(= x_i / l)$

ω Coupled natural circular frequency $(\Omega = \omega / \omega_b)$

ω_b Natural circular frequency parameter $(= \sqrt{EI / \rho_b A l^4})$